



Diffusion in hierarchical silica monoliths: impact of pore size and probe molecule

Alexey Zhokh¹ · Peter Strizhak¹ · Katarzyna Maresz² · Agnieszka Ciemięga² · Julita Mrowiec-Białoń²

Received: 31 December 2019 / Accepted: 22 July 2020 / Published online: 29 July 2020
© Springer-Verlag GmbH Germany, part of Springer Nature 2020

Abstract

The silica monoliths were prepared by a combination of sol-gel synthesis, pore templating, and a process of phase separation. The as-prepared monoliths are characterized by meso- and macroporosity. The pore size significantly differs for each sample depending on the preparation conditions. The transport properties of the monoliths were investigated using benzene, isopropanol, hexane, and methane as probing molecules. The effective diffusion coefficients in the monoliths were estimated based on the second Fick's law of diffusion. The obtained diffusivities are quite similar for different samples, demonstrating that the diffusion occurs mainly in the macropores of the monolith. The values of the diffusion coefficients were found to fall outside the Knudsen prediction. In addition, it was investigated that the benzene and hexane transport in the monolith sample with a bimodal mesopores distribution does not follow the Fick's diffusion law. To describe the mass transfer of the benzene and hexane in this sample the time-fractional diffusion equation was utilized on a phenomenological basis. Several scenarios concerning the role of the relatively small mesopores in the hydrocarbons diffusion are discussed.

1 Introduction

Silica monolithic materials with hierarchical pore size distribution are the objective of research in recent years due to their exceptional properties, i.e. high porosity, large specific surface area and extended continuous network of meso and macropores [1–5]. The monoliths were prepared with the use of the sol-gel process of silicon alkoxide precursor under acidic conditions and phase separation induced by a water-soluble polymer. The composition of the initial reaction mixture and process conditions have impact on the porous structure both in meso and macro scales. A final mesoporous structure of these materials also strongly depended on the post-gelation treatment in an aqueous ammonia solution due

to Ostwald ripening mechanism [6, 7]. The monoliths appeared to be good candidates for application in continuous flow processes e. g. for a chromatographic analysis [8–12], as supports of active species for catalytic and sorption processes and in the fabrication of microreactors [13–19]. In order to meet the expectations for these applications, the monoliths should be characterized by well-defined micrometer-range pores and well-developed mesoporosity. The thickness of the silica skeleton is also of great importance as it determines an effective diffusion path length and time scales. Except a liquid chromatography, the application of monoliths for microreactors fabrications requires the materials with low-pressure drops (<1 bar/cm) [14]. Fortunately, monoliths with large macropores, in the range of 20–50 μm fully meet these requirements and they were successfully obtained [6, 7]. Moreover, the skeletal mesopores providing large specific surface areas allow achieving the high concentration of active sites per unit of volume, which translates directly for high efficacy. The structural properties of the monoliths and their functionalization with various active species were published in numerous papers. The effectiveness of microreactors has been confirmed in important chemical processes, e. g. Diels-Alder reaction [20], Knoevenagel condensation [21], MPV selective reduction of carbonyl compounds [22–25], selective oxidation [26] and in enzyme-catalysed processes [27–29].

Electronic supplementary material The online version of this article (<https://doi.org/10.1007/s00231-020-02929-3>) contains supplementary material, which is available to authorized users.

✉ Alexey Zhokh
al.zhokh@gmail.com

¹ L.V. Pisarzhevskii Institute of Physical Chemistry, National Academy of Sciences of Ukraine, prospect Nauki 31, Kiev 03028, Ukraine

² Institute of Chemical Engineering, Polish Academy of Sciences, Bałtycka 5, 44-100 Gliwice, Poland

To be effectively used as a microreactor, catalyst, or sorbent, a monolith should exhibit low diffusion resistance. In hierarchical materials, the mass transfer scenarios may be significantly different [30]. For instance, the mass transfer in a porous media with a bimodal pore distribution may follow a combination of the diffusion process in each pore geometry [31]. However, it has been found that, for a hierarchical material, an approach based on combining the diffusion process in each pore system overestimates the effective diffusion coefficient [32, 33]. The remarkable deviation of the diffusion length from the pore size has been affirmed in hierarchical zeolite [34]. In addition, the anomalous diffusion that cannot be described by Fick's law has been verified in the porous media [35]. Recent findings concerning the diffusion in a porous medium indicated that the diffusion regime may cross over from the single-file to either two dimensional [36] or to the standard diffusion [37]. This transition has been experimentally verified for various systems, e.g. zeolite membranes [38] and carbon nanotubes [39]. In this respect, the monoliths with a hierarchical porous structure may be characterized by the anomalous diffusion of a molecule. The anomalous diffusion may provide either slower or faster transport compared to the standard diffusion [40, 41]. Therefore, depending on the diffusion regime in the silica monolith process productivity may be either intensified or inhibited.

The unique physicochemical properties of hierarchical silica monolithic materials have been highlighted in the literature. However, so far the diffusion in these materials was studied only numerically, and the impact of the size of tracer particles on long-time effective diffusion coefficient was determined [42]. In this report, the diffusion in hierarchical silica materials was studied experimentally using four probing molecules (benzene, isopropanol, hexane, and methane). It is demonstrated that bimodal mesopore distribution with a significant difference of the pore size governs the deviation from the Fick's diffusion law. In contrast, silica monolith with uniformly distributed mesopores is characterized by standard diffusion. The obtained diffusion coefficients demonstrate very little difference for various monoliths indicating that most of the flux seems to pass through the macropores.

2 Theory

The standard diffusion is usually described by the second Fick's law of diffusion:

$$\frac{\partial C}{\partial t} = D \cdot \frac{\partial^2 C}{\partial x^2} \quad (1)$$

where: C – linear concentration of the diffusing species, mole/cm; D – the diffusion coefficient, cm²/s; t – time, sec; x – space coordinate, cm.

For a description of the diffusion process, which does not follow the Fick's formalism; we use the time-fractional diffusion equation:

$$\frac{\partial^\alpha C}{\partial t^\alpha} = K \cdot \frac{\partial^2 C}{\partial x^2} \quad (2)$$

where: α – the fractional order; K – time-fractional diffusion coefficient, cm²/sec ^{α} . Evidently, the use of the time-fractional diffusion equation is based on the assumption of the time-fractionality of the relevant mass transfer process. Any other non-Fickian diffusion equation may be used for quantification of the obtained experimental results. The time-fractional derivative in Eq. (2) is used according to the Caputo definition [43]:

$$\frac{\partial^\alpha C}{\partial t^\alpha} = \frac{1}{\Gamma(m-\alpha)} \cdot \int_0^t (t-\tau)^{m-\alpha-1} \cdot \frac{\partial^m C}{\partial \tau^m} d\tau \quad (3)$$

where: m – a constant equal to 1 and 2 for $0 < \alpha < 1$ and $1 < \alpha < 2$, respectively; $\Gamma(*)$ – the Euler gamma function.

For the following initial and boundary conditions:

$$C(x, 0) = C_0(x) = \text{const} \quad (4)$$

$$\left. \frac{\partial C}{\partial x} \right|_{x=0} = 0 \quad (5)$$

the solutions of Eqs. (1) and (2) given as the concentration $C(L, t)$ at an upper boundary L , cm, corresponding to the thickness of the grain, may be obtained for the long times using the Green's function approach. For the standard diffusion equation (Eq. (1)) the corresponding long-time solution is given by [44]:

$$C(L, t) = C_0 \cdot A \cdot \exp \left[-\frac{D \cdot t \cdot \pi^2}{L^2} \right] \quad (6)$$

For the time-fractional diffusion equation (Eq. (2)) the corresponding solution at a long time is given by [45]:

$$C(L, t) = C_0 \cdot \frac{L^2 \cdot \sqrt{2 \cdot \pi}}{K \cdot t^\alpha \cdot \Gamma(m-\alpha)} \quad (7)$$

Eqs. (6) and (7) hold for the time decay of concentration in a range that satisfies the following relation: $C(L, t) \leq 0.5 \cdot C_0$ [46], where C_0 is the initial concentration of the diffusing species.

The obtained solutions may be transformed into the logarithmic coordinates. Particularly, for the standard diffusion equation, the corresponding transformation yields:

$$\ln \left[\frac{C(L, t)}{C_0} \right] = -\frac{\pi^2 \cdot D}{4 \cdot L^2} \cdot t + \ln A \quad (8)$$

Whereas for the time-fractional diffusion equation the logarithmic transformation gives:

$$\ln \left[\frac{C(L, t)}{C_0} \right] = -\alpha \cdot \ln t + \ln \left[\frac{4 \cdot L^2}{\Gamma(m-\alpha) \cdot \pi^2 \cdot K} \right] \quad (9)$$

In Eq. (9), the slope directly corresponds to the anomalous diffusion exponent. Contrary, in order to obtain the order of the temporal derivative from the slope, Eq. (8) should be transformed to the logarithmic coordinates as follows:

$$\ln \left[\ln A - \ln \left[\frac{C(L, t)}{C_0} \right] \right] = \ln t + \ln \left[\frac{\pi^2 \cdot D}{4 \cdot L^2} \right] \quad (10)$$

Herein, we treat the one-dimensional forms of the diffusion equations for the sake of computational simplicity. Evidently, this simplification may not be absolutely correct on the physical basis. In this paper, we account only for the diffusant concentration evolution versus time and not the concentration distribution in the volume of the silica monolith. Moreover, we assume that the initial concentration distribution across the monolith is uniform. In the experiment, only the upper surface of the monolith is permeable for the diffusing species. Therefore, we may consider the one-dimensional diffusant flux, i.e. the flux through the upper surface of the silica monolith, whereas the fluxes in the other directions may be neglected. It should be also emphasized that the relevant solution follows the same temporal evolution nevertheless which form of the diffusion equation is used, i.e. one-dimensional or three-dimensional [47].

3 Experimental

Tetraethoxysilane (TEOS, 99%, ABCR), polyethylene glycol (PEG 35000, Sigma Aldrich), nitric acid (65%, Avantor), cetyltrimethylammonium bromide (CTAB, Sigma Aldrich) and ammonia aqueous solution (25%, Avantor Performance Materials) were used for monoliths' synthesis. All the chemicals were used without further purification.

The silica monoliths in the form of rods were synthesized using combined sol-gel, pore templating and phase separation processes described in [6]. Polyethylene glycol (PEG 35000), was dissolved in HNO₃ solution. The mixture was placed in an ice-bath and TEOS was added dropwise after 30 min of stirring cetyltrimethylammonium bromide (CTAB) was added. Next, polypropylene tubes were filled with the sol to obtain monoliths. The samples were stored at 40 °C for gelation and aging. Subsequently, rod-shaped monoliths were washed with an excess of water, treated in ammonia solution, washed again with water and finally calcined in air at 550 °C. Details of the reaction mixture composition and synthesis conditions of monoliths are given in Table 1.

The structural properties of the silica monoliths were characterized by means of several techniques. Specific surface area (S_{BET}), mesopore size distribution and their volume were obtained from nitrogen adsorption data (ASAP 2020 Micromeritics instrument). Macropore structure was analysed by means of mercury porosimetry (Micromeritics Autopore

IV 9510) and scanning electron microscopy (TM 30000 Hitachi). Moreover, skeletal density was measured by a helium pycnometer (AccuPyc 1330) and FTIR spectra were recorded in a Nicolet 6700 spectrometer using DRIFT technique.

The mass transfer experiment was performed using commercial gas chromatograph LHM-72 with the flame-ionization detector. The chromatograph was modified viz. the diffusion cell, which was installed except the chromatography column. The detailed description of the cell working principle, as well as the pellet installation inside the cell in full details, are presented in our referenced study [45]. A sketch of the experimental setup used for the diffusion study is shown in Fig. 1. The monolith grain is placed inside the cell and fixed with inert non-porous sodium silicate. This material is impermeable for the diffusing species. The only upper surface is free for diffusant penetration so that initial and boundary conditions (4)–(5) are satisfied. The following diffusants were used: benzene, isopropanol, hexane, and methane. The experimental conditions were used as follows: diffusant amount manually injected into evaporator was 0.3 μl and 0.6 μl for liquid diffusants (benzene, isopropanol, and hexane), 0.5 ml and 1.0 ml for the gaseous diffusant (methane), temperature inside the diffusion cell was kept 120 °C, gas-carrier (*Ar*) flow was 30 cm^3/min , and thickness of each sample was 0.5 cm.

Benzene, isopropanol, hexane, and methane were used as diffusants since these chemicals are typical reagents of important industrial processes that may be potentially operated in microreactors. Particularly, benzene nitration and hydrogenation may be processed in a microreactor [48, 49]. Photosensitized isopropanol reaction with furanone in a glassy microreactor was reported [50]. Hexane is a usual continuous phase of the processes performed using microreactor technology [51, 52]. Methane partial oxidation in a microreactor is widely used for syngas synthesis [53, 54]. In microreactors, the reactions based on the multiphase gas-liquid systems are usually processed [55]. Therefore, the mass transfer peculiarities of reagents play a crucial role in investigating the microreactor performance in the processes carried out on an industrial scale.

4 Results and discussion

4.1 Monolith characterization

The structural properties of these materials were determined from mercury porosimetry (Fig. 2), nitrogen adsorption (Fig. 3) and helium pycnometry. Moreover, the macropore structure was confirmed by scanning electron microscopy (Fig. 4).

The materials have characteristic bimodal pore structure, i.e. the presence of macropores and mesopores with sizes that

Table 1 Composition of the reaction mixture and synthesis conditions of monoliths

Monolith	Molar ratio					Aging (days)	Ammonia treatment		
	TEOS	PEG	H ₂ O	HNO ₃	CTAB		Conc. (mol/L)	Time (h)	Temp. (°C)
M1	1	0.53	14.3	0.27	0.0275	10	1	8	90
M2	1	0.60	13.9	0.26	0	10	1	24	80
M3	1	0.64	14.8	0.42	0	10	0.1	20	40

strongly depended on the synthesis conditions (Table 1), in particular on the ammonia treatment and the use of the structure-directing compound (CTAB). The monolith M1 differs from M2 and M3 by the presence of small mesopores, ca. 2.5 nm, which originated from CTAB used in the synthesis of that material. These small pores had impact on the value of specific surface area (S_{BET}), which was 50% larger than that of M2 material. Moreover, larger mesopores, with diameter ca. 20 nm, were also present in silica skeleton, similarly as in the M2 material. However, the M3 monolith with medium mesopores (diameter ca. 9 nm) showed the largest specific surface area (652 m²/g). Dramatic differences in macropores size were observed (Fig. 4), i.e. very large macropores in the range of 30–50 μm were founded in the M1 material, while in M2 and M3 macropore size was 6–10 μm and 2–4 μm, respectively.

The synthesis conditions had a minor impact on a skeletal and apparent density, and thus on the porosity of studied materials (Table 2). Only in the case of the M3 monolith, smaller skeletal density was observed that those recorded for M1 and M2. It seems to be that the lower concentration of the ammonia solution and lower temperature during thermal treatment (Table 1) were responsible for a less pronounced Ostwald ripening, and hence the less condensed silica skeleton was obtained. All three monoliths were highly porous materials with porosity ca. 90% and amorphous silica skeleton

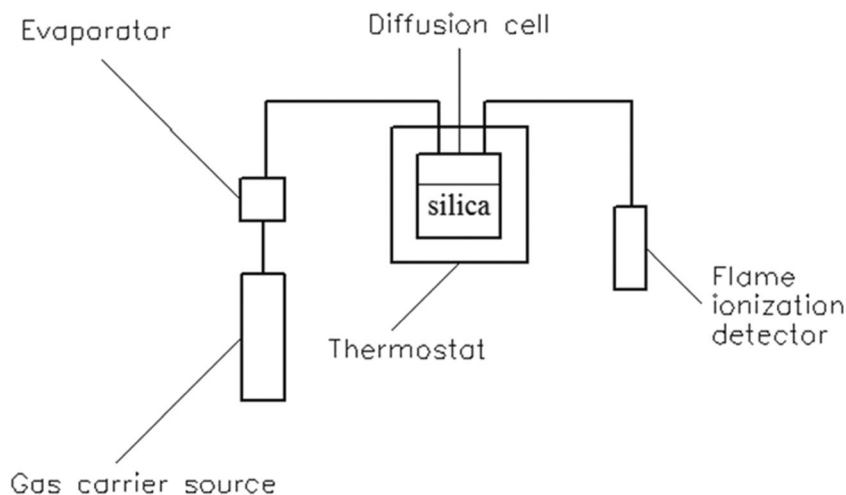
(confirmed by XRD; data not shown here). FTIR spectrum of M1 material was given in Fig. 5. It shows the characteristics absorption band in the range of 3000–3800 cm⁻¹, which corresponds to the stretching vibration of different hydroxyl groups with well seen isolated vicinal SiO-H vibrations at 3750 cm⁻¹. The bands recorded at 1080 and 1220 cm⁻¹ are assigned to Si-O-Si asymmetric stretching modes, while band at 800 cm⁻¹ is associated with symmetric Si-O-Si vibrations.

4.2 Mass transfer investigations

4.2.1 Diffusion regime identification

The mass transfer experiments resulted in the concentration decays on a boundary of a pellet evolving in time. Further, each concentration decay was recalculated into the relative concentration of the corresponding diffusion agent. Fig. S1 of the Supplemental material demonstrates relative diffusant concentration decays for different samples and diffusants. The retention time ranges between approximately 80 and 200 s for liquid diffusants, whereas the retention time for the gaseous diffusant (methane) is considerably lower (15–25 s). The retention time is individual for each diffusant-sample combination, as it follows from the data presented in Fig. S1.

Fig. S2 of the Supplemental material demonstrates an attempt to describe the obtained experimental data by the

Fig. 1 A schematic diagram of the experimental setup

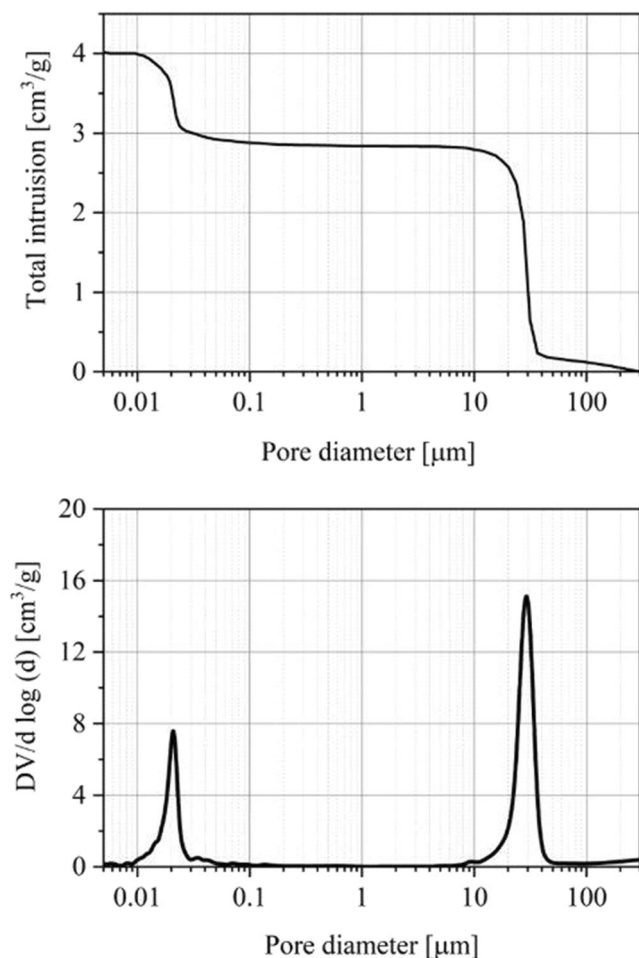


Fig. 2 Cumulative pore volume and pore size distribution vs. pore diameter of M1 monolith determined by mercury porosimetry

solution of the second Fick's law of diffusion. The obtained experimental data are fairly linear while rescaled in the semi-logarithmic coordinates. Furthermore, rescaling the experimental data in the bi-log-log coordinates reveals that the slope is almost equal to unity for all diffusant-porous sample

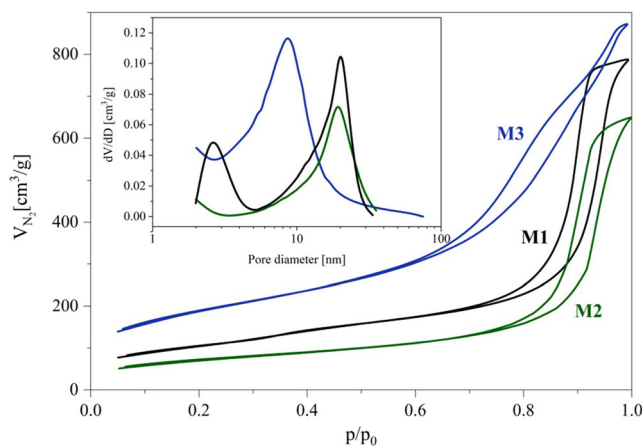


Fig. 3 Nitrogen adsorption and desorption isotherm and pore size distribution (inset)

combinations, except the experimental data for the benzene and the hexane transport through the sample M1. The obtained findings reveal that the methane and isopropanol transport through all the samples, as well as the benzene and the hexane transport through the samples M2 and M3, are standard Fickian. However, the second Fick's law of diffusion fails to describe the experimental data for the benzene and the hexane mass transfer in the sample M1.

Fig. S3 of the Supplemental material shows the experimental data for the benzene and the hexane transport through the sample M1 transformed into logarithmic coordinates according to the time-fractional diffusion model. The correspondence between the experimental data and the solution of the time-fractional diffusion equation is very high. Therefore, the mass transfer of the benzene and hexane through the studied samples is the anomalous one, which may be described by the time-fractional diffusion equation.

4.2.2 Mass transfer parameters

Table 3 gives the measured values of the Fickian diffusion coefficients. The estimated values of the diffusion coefficients are relatively high, comparing to the typical values of the diffusion coefficients in the porous media. However, the porous samples are characterized by the presence of the macroporosity, which may govern the diffusion rate faster than in the geometrically confined media. Moreover, the measured diffusion coefficient increases with the decrease of the diffusant's molecular mass, as they should. The diffusion coefficients exhibit almost no stable trend with respect to the injected diffusant amount. Therefore, it may be concluded the estimated diffusion coefficients are concentration-independent. The diffusion coefficients of the same diffusants measured for different samples are quite similar. To this end, the contribution of the mesopores in the samples to the overall mass transfer rate is lower compared to the contribution of the macropores. Most of the flux seems to pass through the macropores.

Table 4 presents the time-fractional orders and diffusion coefficients for the benzene and hexane transport sample M1. The values of the fractional orders are 1.23 and 1.51 for 0.3 μl and 0.6 μl of the benzene, respectively. The hexane anomalous transport is characterized by the fractional order of 1.16 and 1.19 for 0.3 μl and 0.6 μl diffusant amounts, respectively. For both diffusants, the obtained fractional orders correspond to the superdiffusion, which is faster compared to the standard Fickian diffusion. However, the fractional order seems not to be equal to the anomalous diffusion exponent. For the benzene and hexane transport in the M1 sample, it should be especially emphasized that the experimentally measured values of the anomalous diffusion exponents obtained according to the time-fractional diffusion equation are the effective ones and may not correspond to the real value of the

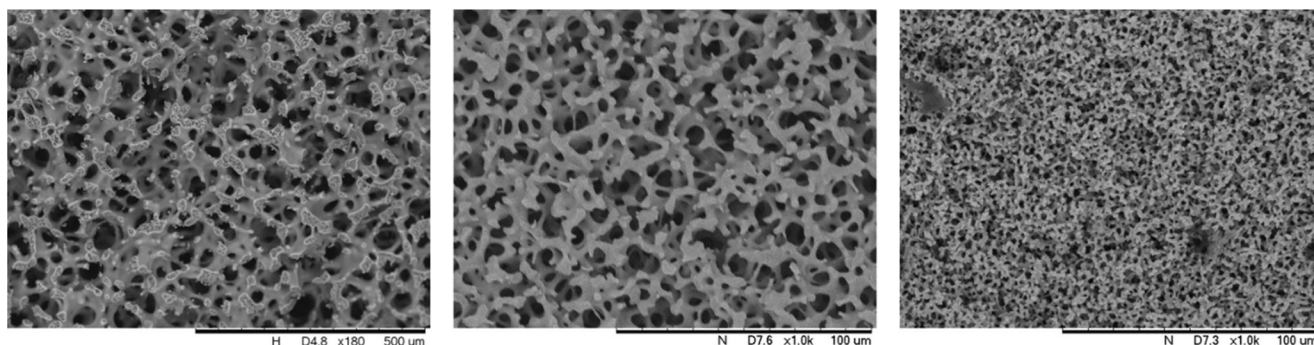


Fig. 4 SEM images of M1, M2 and M3 monoliths (from left to right)

fractional order of the temporal derivative. Particularly, this may reflect a combination of the temporal and spatial fractional orders or be related to the fractal dimension of the environment where the diffusion process occurs.

The time-fractional diffusion coefficients are $0.0309 \text{ cm}^2/\text{s}^\alpha$ and $0.0072 \text{ cm}^2/\text{s}^\alpha$ for $0.3 \mu\text{l}$ and $0.6 \mu\text{l}$ of the benzene, respectively. For the hexane amount of $0.3 \mu\text{l}$, the estimated time-fractional diffusion coefficient is $0.1026 \text{ cm}^2/\text{s}^\alpha$, whereas, for $0.6 \mu\text{l}$ of the hexane, the time-fractional diffusion coefficient equals $0.0904 \text{ cm}^2/\text{s}^\alpha$, as it follows from the data presented in Table 4. To compare the estimated values correctly, their dimensions should be identical. Therefore, a remarkable deviation of the fractional diffusion coefficients for different amounts of the benzene seems to be associated with the difference of the fractional orders. In the porous silica monoliths, large molecules may block some mesopores so that a part of the pore network is not accessible any more [42]. In this respect, increasing the benzene concentration may lead to larger amount of the blocked mesopores. As a result, the benzene mass transfer rate increases giving rise to the time-fractional order. Additionally, different factors may contribute to the observed phenomenon. It may be related to the influence of the porous structure, diffusant concentration, i.e. concentration-dependent transport, capillary condensation in

small mesopores, as well as to their interplay. The diffusion coefficients calculated under the time-fractional diffusion equation are an order of magnitude larger compared to the diffusion coefficients measured in the frame of the standard diffusion model (Table 3). The higher values of the time-fractional diffusivities are governed by different temporal scaling. The time-fractional diffusion model admits the following scaling of the elapsing time: $\sim 1/t^\alpha$, whereas, for the standard Fickian diffusion, the relevant scaling is exponential versus time and may be approximated by $\sim 1/t$ at long times.

4.3 Discussions on process physics

According to the data presented in Figs. 2, 3 and 4, all the silica monolith samples are characterized by the presence of the macropores. The size of the macropores varies between 2 and $50 \mu\text{m}$. The Knudsen theory of the diffusion in porous material states that the pore size influences the mass transfer in the case if the pore size is either lower or identical to the mean free path of a diffusant. The mean free paths of the diffusing species used in the present study are in the range between approximately 30 nm and 85 nm. Therefore, the diffusion process in the macropores is identical to the diffusion in free

Table 2 Structure parameters of materials

Sample	S_{BET} m^2/g	$V_{\text{mezo}}^{\text{a}}$ cm^3/g	$V_{\text{total}}^{\text{b}}$ cm^3/g	$d_{\text{meso}}^{\text{c}}$ nm	$d_{\text{macro}}^{\text{d}}$ μm	$\rho_{\text{s}}^{\text{e}}$ g/cm^3	$\rho_{\text{a}}^{\text{f}}$ g/cm^3	P^{g} %
M1	369	1.20	4.0	2.5/20	30–50	2.229	0.223	90.0
M2	249	0.97	3.7	20	6–10	2.252	0.231	89.7
M3	652	1.34	3.8	9	2–4	2.164	0.244	88.7

^a mesopore volume

^b total pore volume determined by mercury porosimetry

^c mesopore size obtained using BJH method

^d macropore size from mercury porosimetry

^e skeletal density

^f apparent density

^g porosity

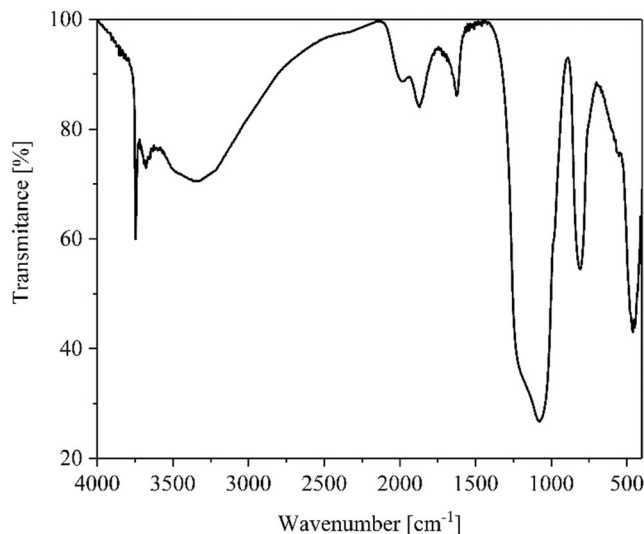


Fig. 5 FTIR spectrum of M1 monolith

Table 3 The values of the diffusion coefficients for each diffusant – porous sample pair

Sample	Diffusant	Diffusant amount	Diffusion coefficient, cm ² /s
M1	Isopropanol	0.3 μl	0.0016
		0.6 μl	0.0023
	Methane	0.3 μl	0.0197
		0.6 μl	0.0163
M2	Benzene	0.3 μl	0.0022
		0.6 μl	0.0023
	Hexane	0.3 μl	0.0028
		0.6 μl	0.0021
	Isopropanol	0.3 μl	0.0030
		0.6 μl	0.0014
	Methane	0.3 μl	0.0201
		0.6 μl	0.0128
M3	Benzene	0.3 μl	0.0019
		0.6 μl	0.0014
	Hexane	0.3 μl	0.0018
		0.6 μl	0.0016
	Isopropanol	0.3 μl	0.0014
		0.6 μl	0.0022
	Methane	0.3 μl	0.0149
		0.6 μl	0.0130

space. In general, the diffusion rate in free space is several orders of magnitude faster compared to the diffusion in a geometrically restricted space, e.g. mesopores or micropores. The diffusion coefficient of the gas in free space is typical of the order of 10^{-1} cm²/sec [56]. The measured diffusion coefficients (Table 3) are obviously much lower compared to the usual diffusion coefficient in free space. Under these considerations, the diffusion in the macropores is not a rate-limiting step of the overall mass transfer process. Transport through the mesopores mainly contributes to the investigated diffusion dynamics. The size of the mesopores for the sample M2 is almost two times larger compared to the sample M3 (Table 2). The diffusion coefficients of almost all diffusants in the sample M2 exhibit higher values than the diffusivities

Table 4 The values of the time-fractional orders and diffusion coefficients for M1 sample

Diffusant	Diffusant amount	Time-fractional diffusion coefficient, cm ² /s ^α	Time-fractional order
Benzene	0.3 μl	0.0309	1.23
	0.6 μl	0.0072	1.51
Hexane	0.3 μl	0.1026	1.16
	0.6 μl	0.0904	1.19

obtained for the sample M3. However, the growth of the diffusion coefficient versus pore size increase does not follow the Knudsen model. To satisfy the Knudsen formalism, the increase of the diffusion coefficient should be equal to an increase in the size of the mesopores, i.e. two times. For the sample M1, the isopropanol diffusion coefficient is quite similar to the sample M3, however, lower than for the sample M2. The rate of the isopropanol transport in the sample M1 with a bimodal mesopore distribution (2.5 nm and 20 nm) is almost identical to the isopropanol diffusion rate through the sample M3 with the size of the mesopores of 9 nm. For the methane diffusion, the diffusion coefficients are approximately equal in the samples M1 and M2, whereas the value of the diffusion coefficient in the sample M3 is remarkably lower. The obtained result demonstrates that the mesopore distribution does not affect the methane mass transfer rate. Only the mesopore size experiences impact on methane diffusion. In contrast, the mesopore distribution influences the mass transfer of the benzene and hexane. The two cases related to the impact of the bimodal pore distribution may be considered. On one hand, the mesopores with the size of 2.5 nm may act as traps for C₆H₆ and C₆H₁₂ molecules in the case if their mass transfer is naturally subdiffusive. On the other hand, provided the benzene and hexane transport is naturally superdiffusive, the movements of the molecules in the small mesopores may correspond to a kind of a retarded ballistic motion with the reduced number of the collisions between the diffusing particles and the pore walls, i.e. so-called sub-ballistic motion.

The measured diffusion coefficients are fairly similar if compared to the literature data. Particularly, the methane diffusivity in the silica almost identical to the values obtained in the present study was estimated using grand canonical Monte Carlo and equilibrium molecular dynamics simulations [57]. The diffusion coefficient of an order of 10^{-6} cm²/sec was obtained by neutron scattering technique for the benzene transport through the microporous silica, as well as it was approved that the Knudsen model fails to predict the value of the benzene diffusion coefficient [58], which is similar to the result derived in the current study. This value is three orders of magnitude lower than the diffusivity measured in the present paper; however, it is not unexpected due to the fact that the pore size of the silica material in this study was an order of magnitude larger. A good correspondence between the obtained results and the data presented in the literature clearly demonstrates the robustness of the performed measurements.

5 Conclusions

The silica monoliths are perfect materials for application as a sorbent, catalyst, and microreactor due to their essential mass transfer properties. The macropores of a silica monolith

provide a transport rate of a diffusing agent, which is identical to a diffusion rate in free space. In this respect, any complications related to the diffusion of a reagent to the surface of a monolith are excluded. In the mesopores of a silica monolith with the size lower than the mean free path of a diffusing species, the obtained diffusivities are of order 10^{-3} cm²/sec and 10^{-2} cm²/sec for a liquid diffusant (at standard conditions) and for a gaseous diffusant (at standard conditions), respectively. The Knudsen diffusion model does not describe the diffusion coefficient change versus the mesopore size increase. For a silica monolith with a bimodal mesopore distribution, the diffusion of C₆ hydrocarbons cannot be described by the second Fick's law of diffusion. As a phenomenological approach, the time-fractional diffusion equation is used to fit the experimental mass transfer kinetics. The origin of the non-Fickian diffusion remains vague, however, it may be attributed to different reasons, e.g. trapping or retarded ballistic in the small mesopores.

Acknowledgments K.M., A.C., and J.M-B acknowledge financial support of the statutory research fund of Institute of Chemical Engineering, Polish Academy of Sciences.

Compliance with ethical standards

Conflict of interests The authors declare no conflict of interests.

References

- Nakanishi K, Takahashi R, Nagakane T et al (2000) Formation of hierarchical pore structure in silica gel. *J Sol-Gel Sci Technol* 17: 191–210. <https://doi.org/10.1023/A:1008707804908>
- Småtå JH, Schunk S, Lindén M (2003) Versatile double-templating synthesis route to silica monoliths exhibiting a multimodal hierarchical porosity. *Chem Mater* 15:2354–2361. <https://doi.org/10.1021/cm0213422>
- El-Safty SA (2011) Instant synthesis of mesoporous monolithic materials with controllable geometry, dimension and stability: a review. *J Porous Mater* 18:259–287. <https://doi.org/10.1007/s10934-010-9390-4>
- Drisko GL, Zelcer A, Caruso RA, Soler-Illia GJ de AA (2012) One-pot synthesis of silica monoliths with hierarchically porous structure. *Microporous Mesoporous Mater* 148:137–144. <https://doi.org/10.1016/J.MICROMESO.2011.08.007>
- Enke D, Gläser R, Tallarek U (2016) Sol-gel and porous glass-based silica monoliths with hierarchical pore structure for solid-liquid catalysis. *Chemie Ing Tech* 88:1561–1585. <https://doi.org/10.1002/cite.201600049>
- Ciemięga A, Maresz K, Malinowski J, Mrowiec-Białoń J (2017) Continuous-flow monolithic silica microreactors with Arenesulphonic acid groups: structure–catalytic activity relationships. *Catalysts* 7:255. <https://doi.org/10.3390/catal7090255>
- Szymańska K, Pietrowska M, Kocurek J et al (2016) Low back-pressure hierarchically structured multichannel microfluidic bioreactors for rapid protein digestion – proof of concept. *Chem Eng J* 287:148–154. <https://doi.org/10.1016/J.CEJ.2015.10.120>
- Tanaka N, Kobayashi H, Nakanishi K et al (2001) Monolithic LC columns. *Anal Chem* 73:420A–429A
- Guiochon G (2007) Monolithic columns in high-performance liquid chromatography. *J Chromatogr A* 1168:101–168. <https://doi.org/10.1016/J.CHROMA.2007.05.090>
- Gritti F, Guiochon G (2012) Measurement of the eddy dispersion term in chromatographic columns. II. Application to new prototypes of 2.3 and 3.2 mm I.D. monolithic silica columns. *J Chromatogr A* 1227:82–95. <https://doi.org/10.1016/J.CHROMA.2011.12.065>
- Hormann K, Müllner T, Bruns S et al (2012) Morphology and separation efficiency of a new generation of analytical silica monoliths. *J Chromatogr A* 1222:46–58. <https://doi.org/10.1016/J.CHROMA.2011.12.008>
- González-Ruiz V, Olives AI, Martín MA (2015) Core-shell particles lead the way to renewing high-performance liquid chromatography. *TrAC Trends Anal Chem* 64:17–28. <https://doi.org/10.1016/J.TRAC.2014.08.008>
- Maresz K, Ciemięga A, Mrowiec-Białoń J et al (2018) Selective reduction of ketones and aldehydes in continuous-flow microreactor—kinetic studies. *Catalysts* 8:221. <https://doi.org/10.3390/catal8050221>
- Galarneau A, Abid Z, Said B et al (2016) Synthesis and textural characterization of Mesoporous and Meso-/macroporous silica monoliths obtained by Spinodal decomposition. *Inorganics* 4:9. <https://doi.org/10.3390/inorganics4020009>
- Guo X, Ding L, Kanamori K et al (2017) Functionalization of hierarchically porous silica monoliths with polyethyleneimine (PEI) for CO₂ adsorption. *Microporous Mesoporous Mater* 245: 51–57. <https://doi.org/10.1016/J.MICROMESO.2017.02.076>
- Chen C, Yang S-T, Ahn W-S, Ryoo R (2009) Amine-impregnated silica monolith with a hierarchical pore structure: enhancement of CO₂ capture capacity. *Chem Commun* 3627. <https://doi.org/10.1039/b905589d>
- Koreniuk A, Maresz K, Odrozek K et al (2015) Highly effective continuous-flow monolithic silica microreactors for acid catalyzed processes. *Appl Catal A Gen* 489:203–208. <https://doi.org/10.1016/J.APCATA.2014.10.047>
- Maresz K, Ciemięga A, Malinowski JJ, Mrowiec-Białoń J (2019) Effect of support structure and polyamine type on CO₂ capture in hierarchically structured monolithic sorbents. *Chem Eng J*:123175. <https://doi.org/10.1016/J.CEJ.2019.123175>
- Galarneau A, Sachse A, Said B et al (2016) Les monolithes silicieux à porosité hiérarchique: une nouvelle classe de microréacteurs pour l'Intensification des procédés en catalyse et en adsorption. *Comptes Rendus Chim* 19:231–247. <https://doi.org/10.1016/j.crci.2015.05.017>
- Sachse A, Hulea V, Finiels A et al (2012) Alumina-grafted macro-/mesoporous silica monoliths as continuous flow microreactors for the Diels–Alder reaction. *J Catal* 287:62–67. <https://doi.org/10.1016/J.JCAT.2011.12.003>
- Sachse A, Galarneau A, Fajula F et al (2011) Functional silica monoliths with hierarchical uniform porosity as continuous flow catalytic reactors. *Microporous Mesoporous Mater* 140:58–68. <https://doi.org/10.1016/J.MICROMESO.2010.10.044>
- Koreniuk A, Maresz K, Mrowiec-Białoń J (2015) Supported zirconium-based continuous-flow microreactor for effective Meerwein–Ponndorf–Verley reduction of cyclohexanone. *Catal Commun* 64:48–51. <https://doi.org/10.1016/J.CATCOM.2015.01.021>
- Ciemięga A, Maresz K, Mrowiec-Białoń J (2018) Meerwein–Ponndorf–Verley reduction of carbonyl compounds in monolithic siliceous microreactors doped with Lewis acid centres. *Appl Catal A Gen* 560:111–118. <https://doi.org/10.1016/J.APCATA.2018.04.037>
- Maresz K, Ciemięga A, Mrowiec-Białoń J (2020) Monolithic microreactors of different structure as an effective tool for in flow

- MPV reaction. *Chem Eng J* 379:122281. <https://doi.org/10.1016/J.CEJ.2019.122281>
25. Ciemięga A, Maresz K, Mrowiec-Białoń J (2017) Continuous-flow chemoselective reduction of cyclohexanone in a monolithic silica-supported Zr(OPri)₄ multichannel microreactor. *Microporous Mesoporous Mater* 252:140–145. <https://doi.org/10.1016/J.MICROMESO.2017.06.023>
 26. Koreniuk A, Maresz K, Odrozek K, Mrowiec-Białoń J (2016) Titania-silica monolithic multichannel microreactors. Proof of concept and fabrication/structure/catalytic properties in the oxidation of 2,3,6-trimethylphenol. *Microporous Mesoporous Mater* 229:98–105. <https://doi.org/10.1016/j.micromeso.2016.04.020>
 27. Szymańska K, Odrozek K, Zniszczoł A et al (2016) MsAcT in siliceous monolithic microreactors enables quantitative ester synthesis in water. *Catal Sci Technol* 6:4882–4888. <https://doi.org/10.1039/C5CY02067K>
 28. Szymańska K, Pudło W, Mrowiec-Białoń J et al (2013) Immobilization of invertase on silica monoliths with hierarchical pore structure to obtain continuous flow enzymatic microreactors of high performance. *Microporous Mesoporous Mater* 170:75–82. <https://doi.org/10.1016/J.MICROMESO.2012.11.037>
 29. Zielińska K, Szymańska K, Mazurkiewicz R, Jarzębski A (2017) Batch and in-flow kinetic resolution of racemic 1-(N-acylamino)alkylphosphonic and 1-(N-acylamino)alkylphosphinic acids and their esters using immobilized penicillin G acylase. *Tetrahedron Asymmetry* 28:146–152. <https://doi.org/10.1016/J.TETASY.2016.11.007>
 30. Schneider D, Kondrashova D, Valiullin R et al (2015) Mesopore-promoted transport in microporous materials. *Chemie Ing Tech* 87:1794–1809. <https://doi.org/10.1002/cite.201500037>
 31. Wang J, Yuan Q, Dong M et al (2017) Experimental investigation of gas mass transport and diffusion coefficients in porous media with nanopores. *Int J Heat Mass Transf* 115:566–579. <https://doi.org/10.1016/j.ijheatmasstransfer.2017.08.057>
 32. Bai P, Haldoupis E, Dauenhauer PJ et al (2016) Understanding diffusion in hierarchical zeolites with house-of-cards Nanosheets. *ACS Nano* 10:7612–7618. <https://doi.org/10.1021/acsnano.6b02856>
 33. Galameau A, Guenneau F, Gedeon A et al (2016) Probing interconnectivity in hierarchical microporous/Mesoporous materials using adsorption and nuclear magnetic resonance diffusion. *J Phys Chem C* 120:1562–1569. <https://doi.org/10.1021/acs.jpcc.5b10129>
 34. Vattipalli V, Qi X, Dauenhauer PJ, Fan W (2016) Long walks in hierarchical porous materials due to combined surface and Configurational diffusion. *Chem Mater* 28:7852–7863. <https://doi.org/10.1021/acs.chemmater.6b03308>
 35. Ergün AN, Kocabaş ZÖ, Yürüm A, Yürüm Y (2014) Diffusion of alcohols and aromatics in a mesoporous MCM-41 material. *Fluid Phase Equilib* 382:169–179. <https://doi.org/10.1016/j.fluid.2014.09.009>
 36. Lucena D, Tkachenko DV, Nelissen K et al (2012) Transition from single-file to two-dimensional diffusion of interacting particles in a quasi-one-dimensional channel. *Phys Rev E* 85:031147. <https://doi.org/10.1103/PhysRevE.85.031147>
 37. Sané J, Padding JT, Louis AA (2010) The crossover from single file to Fickian diffusion. *Faraday Discuss* 144:285–299. <https://doi.org/10.1039/b905378f>
 38. Nelson PH, Auerbach SM (1999) Self-diffusion in single-file zeolite membranes is Fickian at long times. *J Chem Phys* 110:9235–9243. <https://doi.org/10.1063/1.478847>
 39. Chen Q, Moore JD, Liu Y-C et al (2010) Transition from single-file to Fickian diffusion for binary mixtures in single-walled carbon nanotubes. *J Chem Phys* 133:094501. <https://doi.org/10.1063/1.3469811>
 40. Burnecki K, Kepten E, Garini Y et al (2015) Estimating the anomalous diffusion exponent for single particle tracking data with measurement errors - an alternative approach. *Sci Rep* 5:11306. <https://doi.org/10.1038/srep11306>
 41. Metzler R, Klafter J (2000) The random walk's guide to anomalous diffusion: a fractional dynamics approach. *Phys Rep* 339:1–77. [https://doi.org/10.1016/S0370-1573\(00\)00070-3](https://doi.org/10.1016/S0370-1573(00)00070-3)
 42. Hlushkou D, Svidrytski A, Tallarek U (2017) Tracer-size-dependent pore space accessibility and long-time diffusion coefficient in amorphous, Mesoporous silica. *J Phys Chem C* 121:8416–8426. <https://doi.org/10.1021/acs.jpcc.7b00264>
 43. Povstenko Y (2015) Time-fractional thermoelasticity problem for a sphere subjected to the heat flux. *Appl Math Comput* 257:327–334. <https://doi.org/10.1016/j.amc.2014.12.073>
 44. Crank J (1975) *The mathematics of diffusion*, second. Clarendon Press, Oxford
 45. Zhokh A, Strizhak P (2017) Non-Fickian diffusion of methanol in mesoporous media: geometrical restrictions or adsorption-induced? *J Chem Phys* 146:124704. <https://doi.org/10.1063/1.4978944>
 46. Liu JY, Simpson WT (1997) Solutions of diffusion equation with constant diffusion and surface emission coefficients. *Dry Technol* 15:2459–2477. <https://doi.org/10.1080/07373939708917370>
 47. Mandelis A (1995) Green's functions in thermal-wave physics: Cartesian coordinate representations. *J Appl Phys* 78:647–655
 48. Dada EA, Achenie L (2012) Production of Cyclohexane from hydrogenation of benzene using microreactor technology. In: Karimi IA, Srinivasan R (eds) *Computer Aided Chemical Engineering*, 1st edn. Elsevier, Amsterdam, pp 240–244
 49. Burns JR, Ramshaw C (2002) A microreactor for the nitration of benzene and toluene. *Chem Eng Commun* 189:1611–1628. <https://doi.org/10.1080/00986440214585>
 50. Yavorsky A, Shvydkiv O, Nolan K et al (2011) Photosensitized addition of isopropanol to furanones in a continuous-flow dual capillary microreactor. *Tetrahedron Lett* 52:278–280. <https://doi.org/10.1016/j.tetlet.2010.11.018>
 51. Morassutto M, van der Linde P, Schlautmann S et al (2018) Partial reduction of anthracene by cold field emission in liquid in a microreactor with an integrated planar microstructured electrode. *Chem Eng Process Process Intensif* 124:29–36. <https://doi.org/10.1016/j.ccep.2017.10.029>
 52. Wang K, Zhang J, Zheng C et al (2015) A consecutive microreactor system for the synthesis of caprolactam with high selectivity. *AIChE J* 61:1959–1967. <https://doi.org/10.1002/aic.14797>
 53. Mayer J, Fichtner M, Wolf D, Schubert K (2000) A microstructured reactor for the catalytic partial oxidation of methane to syngas. In: *Microreaction technology: industrial prospects*. Springer, Berlin Heidelberg, pp 187–196
 54. Zamaniyan A, Behroozsarand A, Mehdizadeh H, Ghadirian HA (2010) Modeling of microreactor for syngas production by catalytic partial oxidation of methane. *J Nat Gas Chem* 19:660–668. [https://doi.org/10.1016/S1003-9953\(09\)60135-3](https://doi.org/10.1016/S1003-9953(09)60135-3)
 55. Liu Y, Chen G, Yue J (2020) Manipulation of gas-liquid-liquid systems in continuous flow microreactors for efficient reaction processes. *J Flow Chem* 10:103–121
 56. Cussler EL (2009) *Diffusion: mass transfer in fluid systems*. Cambridge University Press, Cambridge
 57. Bhatia SK, Nicholson D (2012) Adsorption and diffusion of methane in silica Nanopores: a comparison of single-site and five-site models. *J Phys Chem C* 116:2344–2355. <https://doi.org/10.1021/jp210593d>
 58. Jobic H, Bee M, Karger J et al (1995) Measurement of the diffusivity of benzene in microporous silica by quasi-elastic neutron scattering and NMR pulsed-field gradient technique. *Adsorption* 1:197–201. <https://doi.org/10.1007/BF00704223>

Publisher's note Springer Nature remains neutral with regard to jurisdictional claims in published maps and institutional affiliations.